

# Revisiting the melting temperature of $\text{NpO}_2$ and the challenges associated with high temperature actinide compound measurements

R. Böhler,<sup>1,2</sup> M. J. Welland,<sup>2</sup> F. De Bruycker,<sup>2,3</sup> K. Boboridis,<sup>2</sup> A. Janssen,<sup>2</sup> R. Eloirdi,<sup>2</sup> R. J. M. Konings,<sup>2</sup> and D. Manara<sup>2,a)</sup>

<sup>1</sup>*Faculty of Applied Sciences, Delft University of Technology, Mekelweg 15, 2629 JB Delft, The Netherlands*

<sup>2</sup>*European Commission, Joint Research Centre, Institute for Transuranium Elements, P.O. Box 2340, 76125 Karlsruhe, Germany*

<sup>3</sup>*Commissariat à l'Energie Atomique, Nuclear Energy Division, Marcoule Research Center, DRCP, 30207 Bagnols sur Ceze, France*

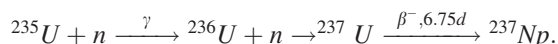
(Received 8 April 2012; accepted 28 April 2012; published online 1 June 2012)

This work revisits the melting behaviour of neptunium dioxide, an actinide compound which can be produced in the nuclear fuel during operation, and which has an important impact on the nuclear fuel and waste radioactivity especially on the very long term. The present experimental approach employs remote laser heating under controlled atmosphere and fast pyrometry. This technique circumvents problems encountered by more traditional heating techniques, in particular, the reaction between sample and containment at temperatures beyond 2500 K. In addition, only a small amount of sample material is required, which is an advantage with respect to the radioactivity and limited availability of neptunium. The  $\text{NpO}_2$  melting/freezing temperature has been measured to be  $3070 \text{ K} \pm 62 \text{ K}$ , much higher than previous values (around 2830 K) obtained by more traditional thermal analysis methods. The large amount of experimental data collected allowed a consistent statistical analysis. It seems likely, although not fully evident from the present results, that the high oxygen potential at temperatures around melting leads to a slightly hypo-stoichiometric congruent melting composition, as already observed in other actinide ( $\text{ThO}_2$ ,  $\text{PuO}_2$ ) and lanthanide oxides (e.g.,  $\text{CeO}_2$ ). Finally, a recently developed phase-field model was used for the simulation of the observed thermograms, allowing a deeper insight in material properties that are difficult to directly measure. For example, a polaron contribution to the high-temperature thermal conductivity, well accepted for the commonly studied actinide oxide  $\text{UO}_2$ , is shown here to likely be present in  $\text{NpO}_2$ .

© 2012 American Institute of Physics. [<http://dx.doi.org/10.1063/1.4721655>]

## I. INTRODUCTION

Neptunium is the first transuranic element. Its most stable isotope,  $^{237}\text{Np}$  (half-life =  $2.144 \times 10^6$  yr), is formed in a nuclear reactor either by  $\alpha$ -decay of  $^{241}\text{Am}$  or by neutron capture of  $^{235}\text{U}$



It is therefore produced as a by-product in nuclear reactors. Due to its long half life, it contributes significantly to the long-term activity of nuclear waste, and is therefore one of the most interesting target nuclides for removal by nuclear transmutation like in the “minor actinide burn-down” or “deep-burn” concepts.<sup>1</sup> Knowledge of properties of Np compounds<sup>2</sup> is therefore important for actinide management technologies, as well as from a fundamental research viewpoint. Particularly, the  $\text{NpO}_2$  melting temperature is important basic information in the actinide dioxide series, which will possibly help, among other aspects, the understanding of the 5f electron behaviour in these compounds.

Two melting point measurements of  $\text{NpO}_2$  were published prior to the present work by Chikalla *et al.*<sup>3</sup> in 1971

and by Richter and Sari<sup>4</sup> in 1987. In both cases, specimens were heated up to the melting point in a resistance furnace and the temperature was measured by pyrometry under blackbody conditions. The melting points reported in these two publications are in excellent agreement,  $2830 \pm 50 \text{ K}$  and  $2820 \pm 60 \text{ K}$ , respectively. Both results may, however, be affected by the high reactivity of the sample, particularly in the liquid phase, at elevated temperature. The present investigation aims at repeating these measurements with an innovative fast heating method, based on high power laser irradiation of the sample coupled with fast multi-channel pyrometry. This method allows the reduction of the heating/cooling duration by orders of magnitude (down to several tens of milliseconds), and the concomitant side effects linked to prolonged high temperatures. Moreover, the atmosphere in which the sample undergoes the solid/liquid phase transition may be controlled. This technique, developed at the European Commission's JRC-ITU in Karlsruhe (Germany), was already successfully used to study the melting behaviour of some actinide compounds like  $\text{PuO}_2$ ,<sup>5</sup>  $\text{UC}$ ,<sup>6</sup>  $\text{UO}_2$ ,<sup>7</sup> whereby the obtained results were sometimes in disagreement with previous literature data based on more traditional heating techniques. This was especially true for oxides, due to their high oxygen potential at temperatures close to melting, whereas the measurements conducted on carbides often yielded results in good agreement with the existing

<sup>a)</sup>Author to whom correspondence should be addressed. Electronic mail: [dario.manara@ec.europa.eu](mailto:dario.manara@ec.europa.eu).

databases. In this context, it appeared that most actinide-oxygen phase boundaries should be revisited, especially at high temperature.<sup>8</sup> It seemed then of great interest to apply the current experimental approach to neptunium dioxide.

A sound interpretation and thorough exploitation of the current experimental temperature vs. time curves were achieved by simulation with a heat transport and a phase-field model. This is an original theoretical approach derived through the theory of irreversible processes.<sup>9</sup>

## II. EXPERIMENTAL PROCEDURE AND MODELLING

### A. Sample preparation

The neptunium dioxide samples were prepared with a mass fraction  $w(^{237}\text{Np})$  of 99.87%, traces of  $^{241}\text{Am}$   $^{238}\text{Pu}$  with mass fractions less than 0.0002% (measured by alpha spectroscopy),  $w(\text{W}) = 0.0276\%$ , and  $w(\text{P}) = 0.05\%$ . The starting material was a powder. Disks 6 mm in diameter and 1.2 to 1.5 mm in thickness were obtained using a bi-directional press. They were then sintered for 8 h in an Ar + H<sub>2</sub> flux at 1973 K with approximately 1500 ppm of H<sub>2</sub>O to densify them, then heat-treated twice in air for 8 h at 1123 K, following Richter and Sari's procedure,<sup>4</sup> and for 12 h at 2000 K just before the laser experiments in order to obtain a composition as close as possible to the exact O/Np = 2 stoichiometry. No weight change was observed after a second annealing, and this was considered a satisfactory test that the stoichiometric composition (O/Np = 2) had been reached.

### B. High temperature measurements

The experimental apparatus used in this work is summarised in Figure 1 and described in detail elsewhere.<sup>10</sup> The sample was mounted in a pressurized cell with a controlled atmosphere inside a  $\alpha$ -shielding glove-box. The contact between the sample and its mount was minimized by using three radially arranged graphite screws to hold the sample in place. The heating agent was a Nd:YAG continuous-wave laser radiating at 1064.5 nm. The laser is programmable with a complex power/time profile of variable duration as short as a few milliseconds and a maximum power of 4.5 kW. Pulses of 70 ms to 720 ms consisted of an initial power ramp, designed to reduce the thermal shock, followed by a constant-power plateau. The sample was heated beyond the melting point and then allowed to cool naturally and resolidify. Such heating cycles were performed under air, air mixed with argon, and Ar + 2% H<sub>2</sub> slightly pressurized up to 0.3 MPa. Quasi-containerless conditions were achieved by

directly heating only a limited area of approximately 3 mm in diameter on the sample surface. The molten volume was therefore contained by the outer periphery of colder solid material, thus, preventing contamination by foreign material. Several experimental parameters could be varied in order to check the impact of the different factors (atmosphere, heating cycle duration, laser spot size, etc.) on the observed melting behaviour.

The surface radiance temperature in the centre of the heated zone was measured by a pyrometer equipped with a fast logarithmic amplifier, operating at 652 nm. The nominal spot size was approximately 0.5 mm in diameter. The pyrometer was calibrated against a standard tungsten-ribbon lamp in the range 1800 K to 2500 K, ensuring traceability to the International Temperature Scale of 1990.<sup>11</sup> The validity of the calibration, the quality of the optical windows, the alignment, and the thermodynamic equilibrium conditions on the measurement spot were tested by measuring *in-situ* the well established melting radiance temperatures of molybdenum, tungsten, and UO<sub>2</sub> (2530 K,<sup>12</sup> 3207 K,<sup>12</sup> and 3040 K,<sup>7</sup> respectively, close to 650 nm).

In addition, a spectro-pyrometer, based on a linear array of 256 photodiodes was used to record the thermal radiance emitted by the sample in the range 550 nm to 920 nm. This instrument allows a spectral analysis, although with a poorer time resolution (one spectrum per millisecond at best). The photodiode at 649 nm was calibrated up to 2500 K using the tungsten-ribbon lamp and this calibration was transferred to a tubular-cavity variable-temperature graphite blackbody-furnace up to 3300 K. The remaining photodiodes were then calibrated with this blackbody, allowing a conversion of their output signal to spectral radiance over the useful wavelength range.

The measured radiance spectra can be fitted in two physically equivalent methods: by a least-squares regression to Planck's distribution law modified by a wavelength- and temperature-dependent function assumed to represent the (near-) normal spectral emittance (NSE),  $\varepsilon(\lambda, T)$ , of NpO<sub>2</sub>, or by the radiance temperature,  $T_r(\lambda)$ , measured during the freezing arrest and plotted as a function of wavelength,  $\lambda$ . The obtained curves were then fitted using Wien's approximation of Planck's law, which is accurate to better than 1% for  $\lambda T < 3100 \mu\text{m K}$

$$\frac{1}{T_r(\lambda)} = \frac{1}{T} - \frac{\lambda}{c_2} \ln \varepsilon(\lambda, T), \quad (1)$$

where  $T$  is the true temperature,  $c_2 = 14\,388 \mu\text{m K}$  is the second radiation constant. If  $\varepsilon$  is independent of wavelength or

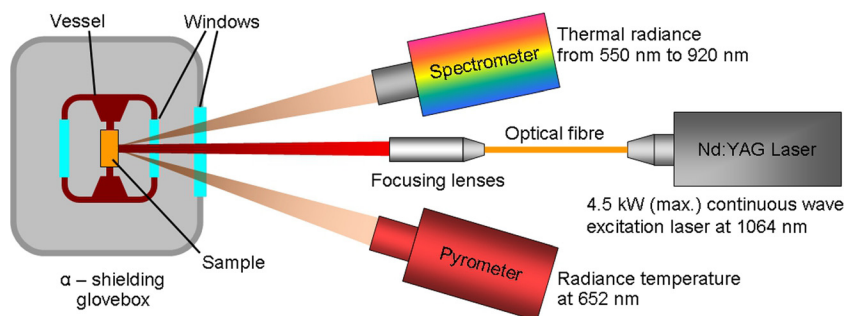


FIG. 1. A scheme of the experimental apparatus used to conduct the melting experiments by laser heating and fast multi-channel pyrometry in the current work.

at least constant at the wavelengths at which  $T_r$  is measured, then plotting  $1/T_r$  as a function of  $\lambda$  results in a straight line fit. When extrapolated to zero wavelength,<sup>13</sup> it intersects the inverse-temperature axis at the inverse true temperature  $1/T$ , as in Eq. (1). In the present work, this approximation of the wavelength-independent NSE (greybody behaviour) resulted in a good fit and was therefore adopted. This is also supported by analogy to emittance data of other similar dioxides (such as  $\text{UO}_2$ , Ref. 14 and  $\text{PuO}_2$ , Ref. 5). In particular, the emittance values thus obtained for liquid and solid  $\text{NpO}_2$  agreed well with those already published for  $\text{UO}_2$  (Ref. 14) and  $\text{PuO}_2$ .<sup>5</sup> The best estimate for the greybody-NSE was then used to convert the measured radiance temperature to true temperatures. Since all measurements were taken on liquid or resolidified material, the surface was considered to be sufficiently smooth, as supported by the good repeatability of the measured radiance temperatures upon freezing.

The melting/freezing temperature of  $\text{NpO}_2$  was determined from the cooling stage of the recorded thermograms, by locating the corresponding thermal arrest. As often observed in rapid laser-heating experiments of such materials, and confirmed by numerical simulation, the heating stage often occurs too quickly to reveal an observable melting arrest during this phase of the thermal cycle.

### C. Material analysis

$\text{NpO}_2$  samples were analyzed by x-ray diffraction (XRD) on the unmolten and resolidified areas with a diffractometer (Cu  $K\alpha_1$  radiation), using a range  $10^\circ$ – $120^\circ$  with 0.009 steps.

Secondary electron (SE) and backscattered electron (BSE) images were recorded on a scanning electron microscope (SEM) operated at 25 kV.

### D. Numerical simulation

Experimental heating cycles were simulated using a phase-field model to account for the phase change. The model determines the thermal transport coupled with phase stability through a phase-field model which tightly links the kinetic model to equilibrium thermodynamic treatments of the material. Similar models were previously used on thermograms from  $\text{UO}_{2+x}$ , which melt non-congruently.<sup>15</sup>

The phase-field model introduces a scalar state variable  $\phi$  representing the fraction of the stable phase at each physical point of the system (e.g.,  $\phi = 1$  for the liquid,  $\phi = 0$  for the solid,  $\phi \in (0,1)$  for a coexistence of the two). This approach permits a versatile description of the system including representation of phase boundaries with diffuse interfaces, whereas its main drawback is large computational expense, resulting in long calculation times.

The model is described in Eqs. (2) and (3) and was implemented in the finite element method software, COMSOL Multiphysics®

$$\underbrace{\rho c_p \frac{DT}{Dt}}_{\text{Energy due to temperature increase}} = - \underbrace{\rho h_{\text{fus}} \frac{D\phi}{Dt}}_{\text{Latent heat of phase change}} - \underbrace{\nabla \cdot \vec{q}}_{\text{Heat conduction}}, \quad (2)$$

$$\underbrace{\frac{D\phi}{Dt}}_{\text{Rate of phase change}} = - \underbrace{\frac{M_\phi}{T}}_{\text{Interface kinetics}} \left( - \underbrace{\rho \frac{h_{\text{fus}}}{T_{\text{fus}}} (T - T_{\text{fus}})}_{\text{Approximate change in entropy at constant volume}} + \underbrace{\frac{\partial K(\phi)}{\partial \phi} - \xi^2 \nabla^2 \phi}_{\text{Interface shaping terms}} \right), \quad (3)$$

where  $c_p$  represents the constant pressure heat capacity,  $\rho$  is the density,  $q$  is the conductive heat flux,  $h_{\text{fus}}$  is the enthalpy of fusion,  $M_\phi$  is the interface attachment kinetic parameter,  $T_{\text{fus}}$  is the temperature of fusion, and  $K$  and  $\xi$  are interface shaping terms required by the phase-field model. Thermal boundary conditions are laser absorption and radiative heat loss. Heat transport in the buffer gas was modelled simultaneously to account for heat loss from the sample.

Many of the material parameters required as input for the model are unknown, especially at the very high temperatures encountered at the liquid state. Missing parameters were therefore extrapolated from lower temperatures or taken from  $\text{UO}_2$  when no other information was available. The enthalpy of fusion was calculated using Richard's law.<sup>16–18</sup> The material properties used are listed in Table I.

Preliminary simulations revealed a discrepancy with the experimental data, which motivated a deeper investigation of the material properties. An important point was noted in the

high temperature thermal conductivity of  $\text{NpO}_2$ , which exhibited a downward trend with increasing temperature, whereas  $\text{UO}_2$  and MOX typically show an upswing due to polarons.<sup>22,23</sup> Upon deeper examination, experiments on the thermal conductivity of  $\text{NpO}_2$  were performed only up to 1473 K (Ref. 21) and show a decreasing trend with temperature, in qualitative agreement with molecular dynamics calculations up to 2200 K.<sup>19</sup> However, the calculations only consider lattice terms, and the measurements are below the threshold of significant polaron contribution in  $\text{UO}_2$ . Therefore, we add the  $\text{UO}_2$  polaron term<sup>20</sup> to the lattice terms for the thermal conductivity of  $\text{NpO}_2$ .

## III. RESULTS

### A. Laser heating

Two  $\text{NpO}_2$  disks were investigated in the present work. When the sample broke into pieces during the experiment,

TABLE I. Material properties used as input parameters in the simulation. The term in angled brackets in the solid thermal conductivity is the polaron terms added as discussed in the text.

Material property	Unit	Value	Reference
Density at 293 K	kg m <sup>-3</sup>	11192.8	Sobolev <sup>18</sup>
Enthalpy of fusion	J mol <sup>-1</sup>	77320	This work
Heat capacity solid	J mol <sup>-1</sup> K <sup>-1</sup>	$11.4 + 1.59 \cdot 10^{-1}(T/K) - 1.33 \cdot 10^{-4}(T/K)^2 + 5.21 \cdot 10^{-8}(T/K)^3 - 6.67 \cdot 10^{-12}(T/K)^4$	Kurosaki <sup>19</sup>
Heat capacity liquid	J mol <sup>-1</sup> K <sup>-1</sup>	$\frac{1.3288 \times 10^9}{(T/K)^2} + 0.25136$	Fink <sup>20</sup>
Absorptivity		0.829	This work
Emissivity		0.829	This work
Thermal conductivity solid	W m <sup>-1</sup> K <sup>-1</sup>	$\frac{1}{0.09447 + 1.797 \cdot 10^{-4}(T/K)} + \left\langle \frac{2.024 \times 10^{11}}{(T/K)^3} e^{\frac{-16350}{(T/K)}} \right\rangle$	Nishi <sup>21</sup>
Thermal conductivity liquid	W m <sup>-1</sup> K <sup>-1</sup>	2.6	Sheindlin <sup>27</sup>

suitably large fragments were also used as further specimens. In total, more than 40 laser heating experiments were carried out, allowing a meaningful statistical analysis of the results. A clear solidification arrest was detected in a well reproducible temperature range, both over many successive shots on the same specimen and on different samples (Figure 2). No indication of segregation or non-congruent evaporation was detectable from such thermal analysis only. Freezing plateaus were sometimes preceded by a dip in temperature as a consequence of undercooling at the surface of the sample which was reproduced in simulations described below.

The near-normal spectral emittance of freezing NpO<sub>2</sub> derived by multi-channel pyrometry using “extrapolation to zero wavelength” is reported in Figure 3. The radiance temperature spectrum, recorded during the freezing arrest with an integration time of 2 and 4 ms, is well fitted with a greybody (constant) emissivity of 0.829. An emissivity uncertainty of 0.08 (at the two standard deviation level) combined with the

data spread and the temperature scale uncertainty ( $\pm 10$  K) yields a NpO<sub>2</sub> freezing temperature of  $3070 \text{ K} \pm 62 \text{ K}$ . Such a temperature was observed to be reproducible, within the given uncertainty limits, over 31 experiments.

By varying the atmosphere and the laser pulse power, no systematic variations of the melting point were observed as shown in Figure 4. All these effects have therefore been taken into account in defining the aforementioned uncertainty bands associated with the current results.

B. Material characterization

The determination of possible permanent composition changes in the samples during the thermal cycles constituted a difficult part of the current investigation. Since no systematic effect linked to a variation of the O/Np ratio could be inferred from the thermal analysis of successive shots, other techniques were employed. Among them, the most consistent

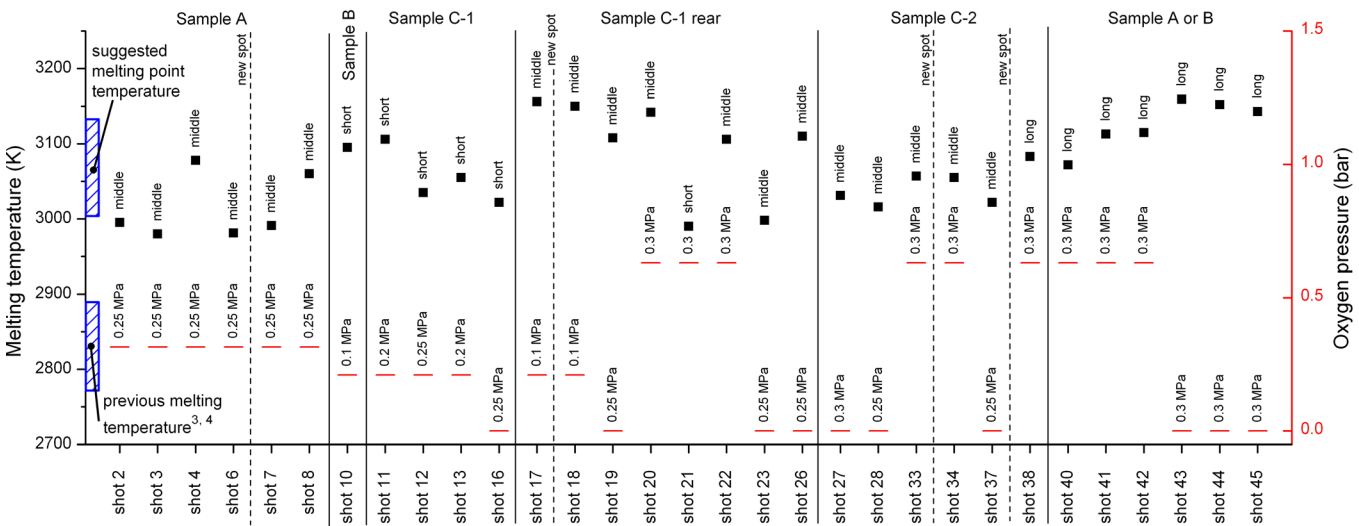


FIG. 2. An overview of all the solidification points measured in NpO<sub>2</sub> samples in this work, together with the partial oxygen pressure and the total pressure set in each experiment. The missing laser irradiation experiments were not taken into consideration for the statistics, but still had an effect on the morphology of the sample surface. Several shots were performed on the same spot on each sample. The experiments are categorized according to the total heating duration (short:  $t < 100$  ms, middle:  $100 \text{ ms} \leq t \leq 150$  ms, long:  $t > 150$  ms). Older literature values of the NpO<sub>2</sub> melting temperature with their uncertainties are compared with the result found in this work ( $3070 \text{ K} \pm 62 \text{ K}$ ).



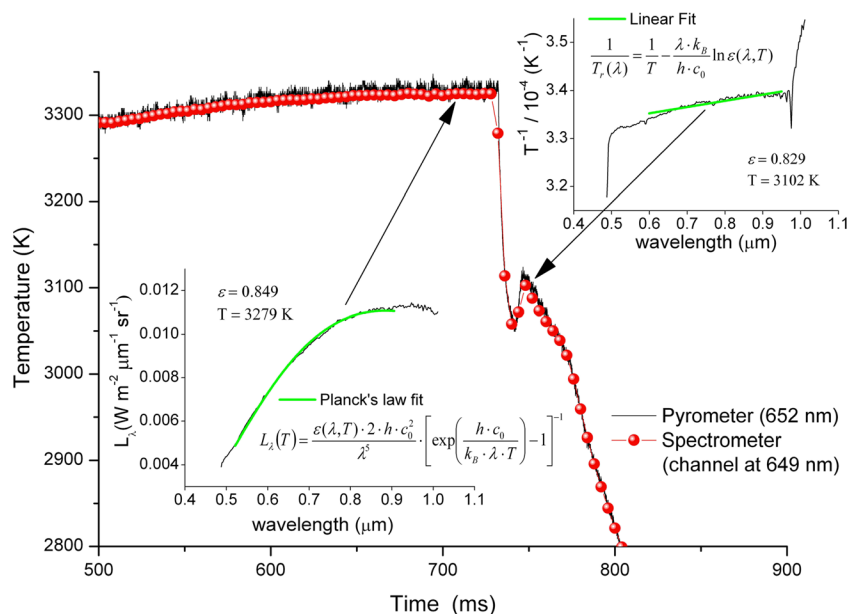


FIG. 3. Typical thermograms recorded at 649 nm (full circles) and 652 nm (solid line) on a laser heated  $\text{NpO}_2$  sample (shot 42) by the spectro-pyrometers used in this work, using an average constant emissivity  $\epsilon = 0.829$ . The two insets show examples of radiance analysis. The first displays a Planck's law fit of an experimental radiance ( $L_2$ ) spectrum recorded in liquid  $\text{NpO}_2$ . The second reports a linear fit derived from Planck's law (Wien's approximation) of the inverse radiance temperature ( $T_r^{-1}$ ) vs. wavelength observed at the  $\text{NpO}_2$  solidification arrest. Both fits were performed, with temperature and emissivity as free parameters, in wavelength domains limited by the acceptability of the signal-to-noise ratio in the experimental curve. In both cases, a good fit was obtained with emissivity independent of temperature and wavelength (gray body behaviour).  $c_0$  = speed of light in vacuum;  $h$  = Planck's constant;  $k_B$  = Boltzmann's constant.

seemed to be XRD, essentially because the dependence of the fcc- $\text{NpO}_{2-x}$  lattice parameter on  $x$  has already been assessed for  $0 \leq x \leq 0.04$  by Richter and Sari.<sup>4</sup> No clear differences were observed between the diffraction of molten/refrozen neptunium dioxide and that of a not molten sample. The resulting lattice parameters were  $(5.435 \pm 0.002)$  Å and  $(5.436 \pm 0.002)$  Å, respectively. This corresponds with Richter and Sari<sup>4</sup> for a composition of  $\text{NpO}_{1.995 \pm 0.010}$  for the molten and  $\text{NpO}_{1.990 \pm 0.010}$  for the non-molten part. These values are very close to the suggested stoichiometric lattice parameter of 5.434 Å in the investigation of Richter and Sari,<sup>4</sup> but a slightly lower O/Np ratio cannot be excluded. Other measurements of the lattice parameter suggest, nevertheless, a value of 5.4333 Å,<sup>24</sup> so that the dependence of the composition has to be revisited.

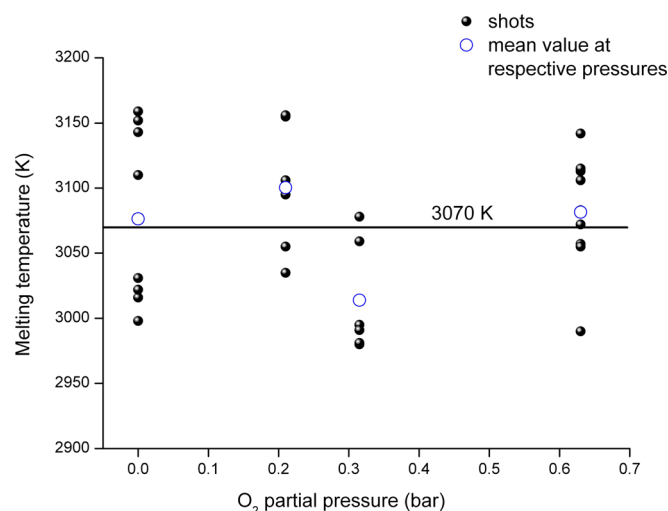


FIG. 4. An overview of the currently measured  $\text{NpO}_2$  solidification temperatures as a function of the  $\text{O}_2$  partial pressure set in the buffer gas. The large empty circles represent the average solidification temperature determined at each oxygen partial pressure. The solid horizontal line represents the overall average solidification temperature.

The fact that samples were nearly stoichiometric both before and after laser irradiation was qualitatively confirmed also by SEM analysis. The electron microscope employed in the BSE mode revealed a clean surface throughout the sample, both in the molten/refrozen and in the unmolten regions, without any precipitations of metallic neptunium (Figure 5), as found by Richter and Sari<sup>4</sup> in hypostoichiometric samples. From a morphological viewpoint, micrographs show that the depth of the molten zone was of the order of some tens of micrometers, and it can be separated from the bulk material by a crack parallel to the surface as shown in Figure 6.

### C. Simulations

The simulated thermogram presented in Figure 7 was computed with a 1D model of shot 22, for which the solidification temperature was recorded at 3100 K. Inputting the experimental laser power vs. time profile and using the

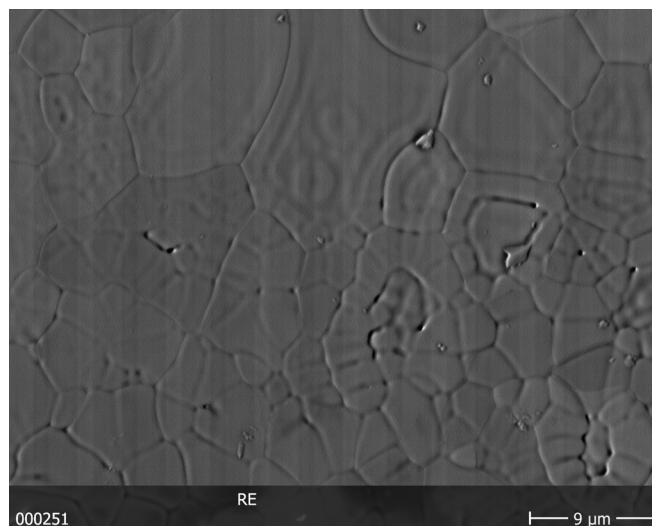


FIG. 5. SEM back scattered electron image of a molten and refrozen  $\text{NpO}_2$  surface. The image shows a homogeneous surface where no second phases, especially metallic Np,<sup>4</sup> can be distinguished by the contrast.

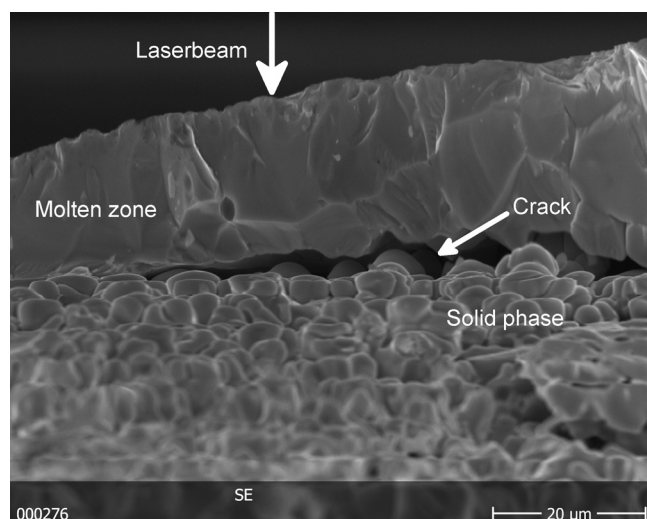


FIG. 6. A SEM cross section image of  $\text{NpO}_2$  laser-melted and refrozen. The surface molten part is clearly detached from the unmolten material underneath by a radial fracture (crack). This kind of cracks can have an important impact on the heat diffusion across of the sample, as they reduce the thermal conductivity.

material properties listed in Table I, the calculated temperature evolution follows qualitatively well with the observed temperatures. The insets in Figure 7 show the temperature and phase profiles at the indicated times as functions of depth into the material. The phase profile at 304 ms corresponds well to the depth of the refrozen liquid observed by SEM on a cross section of the sample as shown in Figure 7.

The difference in the cooling behaviour following the pulse is primarily attributed to the presence of cracks in the sample, generated by thermal stresses during heating and cooling. The cracks retard heat transport away from the surface, thus, slowing the apparent surface cooling rate.

Considering the uncertainty in the majority of the material properties, the thermogram is reasonably well reproduced, indicating that the properties used, including the

polaron term in the thermal conductivity, are at least indicative of their correct values.

#### IV. DISCUSSION

The melting/freezing temperature observed by laser heating on  $\text{NpO}_2$ ,  $3070 \text{ K} \pm 62 \text{ K}$ , is more than 200 K higher than the value reported by Chikalla<sup>3</sup> and Richter and Sari.<sup>4</sup> These latter results were obtained by using traditional heating methods (resistance furnaces) with which the  $\text{NpO}_2$  sample could extensively react with the tungsten containment during the long dwelling time (minutes) at high temperature. On the other hand, in the current work the apparent melting/freezing point did not increase when performing repeated or longer experiments under oxidizing conditions. Since none of the techniques used to characterize the molten/refrozen material at room temperature gave evidence of any oxygen losses, except the XRD which indicated the possibility of a very slight hypostoichiometry both in the fresh and the laser irradiated materials, it can be concluded that neptunium dioxide melts congruently at a composition of  $1.98 \leq \text{O/Np} \leq 2$ . This agrees fairly well with available thermodynamic assessment of the Np–O phase diagram,<sup>4,25</sup> although the current investigation reveals a much higher melting temperature. Both the extent of the reported uncertainty band ( $\pm 62 \text{ K}$ ) and the (much larger) difference between the current results and the previous literature data give an idea of the experimental difficulties inherent in the high-temperature investigation of chemically reactive materials like  $\text{NpO}_2$ .

The qualitative agreement between the experimental and simulated thermograms is acceptable in that the main features of the process are reproduced. The approach constitutes a valuable tool yielding a deeper picture of heating/melting and the cooling/freezing process. In the absence of a flat temperature plateau during solidification, the simulation confirms and explains why the maximum temperature observed is the true freezing temperature of the material.

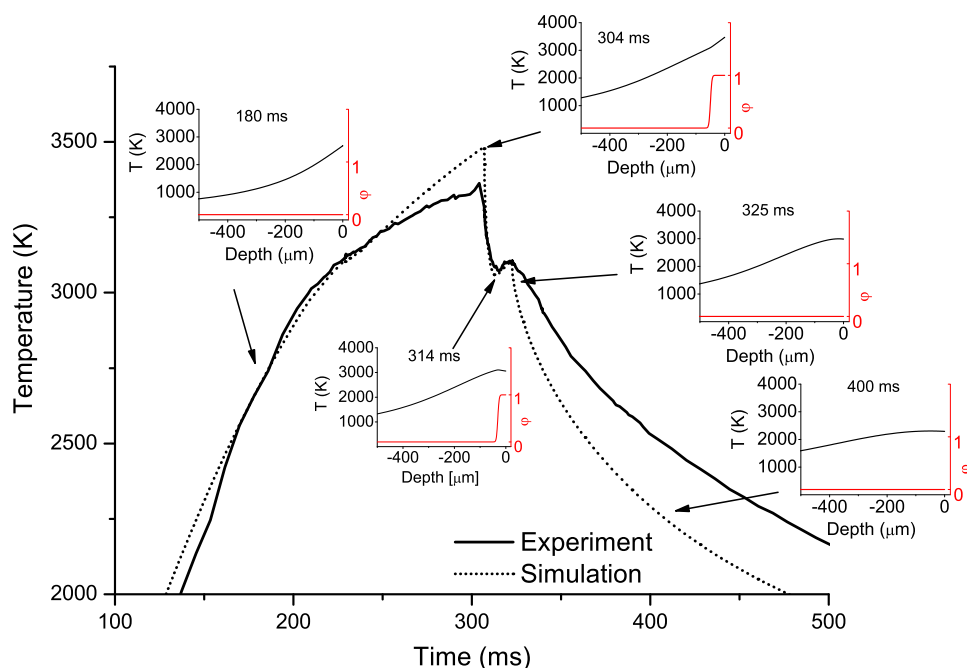


FIG. 7. Comparison between an experimental thermogram (solid black line) recorded on a  $\text{NpO}_2$  specimen laser-heated beyond melting (shot 22) and a calculated thermogram (dotted line) obtained from the 1-dimensional phase-field simulation of the same experiment. The insets show the temperature ( $T$ ) and phase-field parameter ( $\phi$ ) as a function of depth at different time points during the heating-cooling cycle. In each inset, the region with  $\phi = 0$  corresponds to solid and the one with  $\phi = 1$  to liquid neptunium dioxide. The solid/liquid interface domain is characterized by intermediate values:  $0 < \phi < 1$ .

Another value of the simulation is the strong indication that polarons are present and contribute significantly to the thermal conductivity at high temperatures. With suitable development, the treatment may be used in the inverse problem for material parameter estimation (e.g., the thermal conductivity of liquid  $\text{NpO}_2$ ).

In the end, devising a comprehensive approach (both experimental and theoretical) to obtain a satisfactory picture of all phenomena occurring under extreme experimental conditions constitute the main research challenges in the field of high temperature thermodynamics. This level of understanding is also of paramount importance for the analysis of accidental conditions which can be produced, for example, in a nuclear reactor or in nuclear waste during thermal excursions when insufficient cooling is provided.

Once more, a situation similar to that already observed elsewhere for  $\text{CaO}$ ,<sup>26</sup>  $\text{CeO}_2$ ,<sup>27</sup>  $\text{UO}_{2+x}$ ,<sup>7</sup> and  $\text{PuO}_2$  (Ref. 5) is reproduced here: the reaction between the sample and its environment, enhanced by exchange of oxygen, probably leads to an apparent freezing temperature very different from the one measured for the well-controlled and well-contained material. The result is of great importance with respect to the behaviour of this sort of oxides, and highlights the impact of temperature and atmosphere on it.

The new value of the melting/solidification temperature for  $\text{NpO}_2$  fits well in between the values for its neighboring actinide oxides ( $\text{UO}_2$ ,  $\text{PuO}_2$ ). However, the general trend of the entire actinide dioxide series, reported in Figure 8,<sup>3,5,7,28–31</sup> changes considerably when new values for  $\text{NpO}_2$  and  $\text{PuO}_2$  are taken into account instead of old ones. Figure 8 also shows that the difference between old and new melting temperatures of actinide dioxides increases with the atomic number of the actinide. More importantly, this difference seems to increase

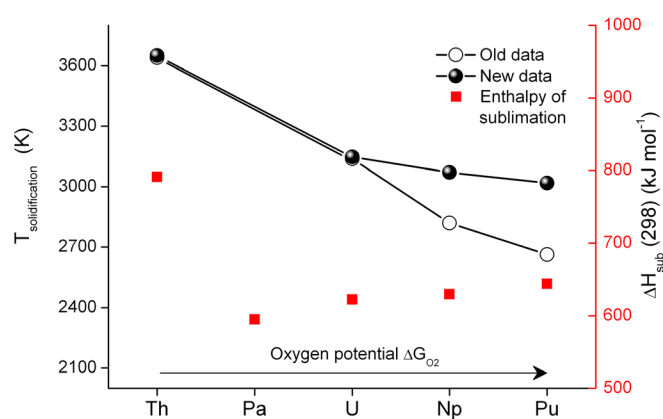


FIG. 8. Comparison between old (induction furnace heating in a tungsten crucible)<sup>3,29–31</sup> and new (quasi-containerless laser heating)<sup>5,7,28</sup> data points for the melting/solidification temperatures of dioxides of the actinide series. Data for the dioxides of protactinium and trans-plutonium actinides are missing or considered as unreliable. The difference between new and old data points increases with the atomic number of the actinide and the oxygen potential<sup>32</sup> of the corresponding dioxide. Data of the room temperature sublimation enthalpy  $\Delta H_{\text{sub}}(298)$ <sup>33–37</sup> for the actinide dioxide series are also reported for comparison. Similar to the melting/solidification temperature trend,  $\Delta H_{\text{sub}}(298)$  is much higher for  $\text{ThO}_2$  than for the other actinide dioxides, signifying a correspondingly larger cohesion energy of thorium dioxide, which has no f-electrons involved in the formation of molecular orbitals.

with the oxygen potential of the respective dioxide at a given temperature.<sup>32</sup> This shows the suitability of the current approach for the investigation of these materials, particularly in the cases where they display a strong tendency to exchange oxygen with their environment.

It is finally interesting to compare the qualitative behaviour of the room temperature sublimation enthalpy  $\Delta H_{\text{sub}}(298)$  (Refs. 33–37) for the actinide dioxide series with the newly assessed melting/freezing points of the same compounds.  $\Delta H_{\text{sub}}(298)$  is in fact known to be much higher for  $\text{ThO}_2$  than for the other actinide dioxides (Figure 8), signifying a correspondingly larger cohesion energy of thorium dioxide, which has no f-electrons involved in the formation of molecular orbitals. This suggests that new experimental data like the current ones might help a better comprehension of the f-electron behaviour in actinide compounds. Moreover, such behaviour parallels the reported melting/freezing points consistently, and encourages further research in this fascinating domain. For example, even the solid/liquid transition temperature of protactinium dioxide can be estimated to be close to the one of  $\text{UO}_2$  if the current trend is proven to be correct.

## V. CONCLUSIONS

The melting behaviour of  $\text{NpO}_2$  has been revisited in this work by means of fast remote laser heating under controlled atmosphere. The following conclusions can be drawn from the present research:

- Neptunium dioxide melts at  $(3070 \pm 62)$  K, at a composition between  $\text{NpO}_{1.98}$  and  $\text{NpO}_{2.00}$ .
- Although it is likely that stoichiometric  $\text{NpO}_2$  undergoes oxygen losses before melting, no clear effect of the external atmosphere on the liquid/solid transition could be observed in the current work, where a composition close to stoichiometric was maintained, thanks to the short material exposure at high temperature.
- Large disagreement ( $>200$  K) between the current results and earlier experimental data obtained by W-furnace heating shows that the melting behaviour of neptunium dioxide is largely determined by the interaction between this material and its containment, essentially due to the high oxygen potential of  $\text{NpO}_2$ ; a similar behaviour had already been observed for other similar compounds (e.g.,  $\text{CeO}_2$ ,  $\text{PuO}_2$ ).
- Phase-field simulations of the current experiments give good insight into the phenomena occurring during the laser heating cycles.
- Comparison between experimental and simulated thermograms reveals that the high-temperature thermal conductivity of  $\text{NpO}_2$  likely behaves similarly to  $\text{UO}_2$ , where the polaron contribution plays an essential role.
- The melting point trend of actinide dioxides as a function of the actinide atomic number  $Z$  can be reassessed with the current data: this trend seems to qualitatively resemble that of the sublimation enthalpies for the same compounds. Thanks to correlations of this type, the melting point of so far unmeasured compounds might be estimated.

These encouraging results motivate further research on the very high temperature behaviour of other materials, whose behaviour might result considerably more complex than it could be believed on the basis of traditional furnace heating experiments only.

- <sup>1</sup>C. Rodriguez, *Nucl. Eng. Des.* **222**, 299 (2003).
- <sup>2</sup>R. J. Lemire, J. Fuger, H. Nitsche, P. Potter, M. H. Rand, J. Rydberg, K. Spahiu, J. C. Sullivan, W. J. Ullman, P. Vitorge, and H. Wanner, *Chemical Thermodynamics of Neptunium and Plutonium*, Chemical Thermodynamics Series Vol. **4**, 4th ed. (Elsevier, 2001).
- <sup>3</sup>T. D. Chikalla, C. E. McNeilly, J. L. Bates, and J. J. Rasmussen, "High-Temperature Phase Transformations in Some Lanthanide and Actinide Oxides," Battelle North-West Laboratory Report - SA 3818, September, 1971.
- <sup>4</sup>K. Richter and C. Sari, *J. Nucl. Mater.* **148**, 266 (1987).
- <sup>5</sup>F. De Bruycker, K. Boboridis, P. Pöml, R. Eloiardi, R. J. M. Konings, and D. Manara, *J. Nucl. Mater.* **416**, 166 (2011).
- <sup>6</sup>C. A. Utton, F. De Bruycker, K. Boboridis, R. Jardin, H. Noel, C. Guéneau, and D. Manara, *J. Nucl. Mater.* **385**, 443 (2009).
- <sup>7</sup>D. Manara, C. Ronchi, M. Sheindlin, M. Lewis, and M. Brykin, *J. Nucl. Mater.* **342**, 148 (2005).
- <sup>8</sup>C. Guéneau, N. Dupin, B. Sundman, C. Martial, J.-C. Dumas, S. Gossé, S. Chatain, F. D. Bruycker, D. Manara, and R. J. M. Konings, *J. Nucl. Mater.* **419**, 145–167 (2011).
- <sup>9</sup>S. R. D. Groot and P. Mazur, *Non-Equilibrium Thermodynamics* (Dover, 1985).
- <sup>10</sup>D. Manara, M. Sheindlin, W. Heinz, and C. Ronchi, *Rev. Sci. Instrum.* **79**, 113901 (2008).
- <sup>11</sup>H. Preston-Thomas, *Metrologia* **27**, 3 (1989) (amended version).
- <sup>12</sup>R. E. Bedford, G. Bonnier, H. Maas, and F. Pavese, *Metrologia* **33**, 133 (1996).
- <sup>13</sup>A. S. Tenney, "Radiation ratio thermometry," in *Theory and Practice of Radiation Thermometry*, edited by D. P. DeWitt and G. D. Nutter (Wiley, Hoboken, NJ, USA, 1988).
- <sup>14</sup>M. Bober, J. Singer, and K. Wagner, *Spectral Reflectivity and Emissivity Measurements of Solid and Liquid UO<sub>2</sub> at 458, 514.5 and 647 nm as a Function of Polarization and Angle of Incidence* (Kernforschungszentrum Karlsruhe, 1980).
- <sup>15</sup>M. J. Welland, W. T. Thompson, B. J. Lewis, and D. Manara, *J. Nucl. Mater.* **385**, 358 (2009).
- <sup>16</sup>P. Papon, J. Leblond, and P. H. E. Meijer, *The Physics of Phase Transitions*, 2nd ed. (Springer, Berlin, 2002).
- <sup>17</sup>L. F. Epstein, *J. Nucl. Mater.* **22**, 340 (1967).
- <sup>18</sup>V. Sobolev, *J. Nucl. Mater.* **344**, 198 (2005).
- <sup>19</sup>K. Kurosaki, M. Imamura, I. Sato, T. Namekawa, M. Uno, and S. Yamana, *J. Alloys Compd.* **387**, 9 (2005).
- <sup>20</sup>J. Fink, *J. Nucl. Mater.* **279**, 1 (2000).
- <sup>21</sup>T. Nishi, A. Itoh, M. Takano, M. Numata, M. Akabori, Y. Arai, and K. Minato, *J. Nucl. Mater.* **376**, 78 (2008).
- <sup>22</sup>M. Sheindlin, D. Staicu, C. Ronchi, L. Game-Arnaud, B. Remy, and A. Degiovanni, *J. Appl. Phys.* **101**, 093508 (2007).
- <sup>23</sup>J. J. Carbajo, G. L. Yoder, S. G. Popov, and V. K. Ivanov, *J. Nucl. Mater.* **299**, 181 (2001).
- <sup>24</sup>D. Taylor, *Br. Ceram. Trans. J.* **83**, 32 (1984).
- <sup>25</sup>H. Kinoshita, D. Setoyama, Y. Saito, M. Hirota, K. Kurosaki, M. Uno, and S. Yamanaka, *J. Chem. Thermodyn.* **35**, 719 (2003).
- <sup>26</sup>T. Yamada, M. Yoshimura, and S. Somiya, *J. Am. Ceram. Soc.* **69**, C-243 (1986).
- <sup>27</sup>M. Zinkevich, D. Djurovic, and F. Aldinger, *Solid State Ionics* **177**, 989 (2006).
- <sup>28</sup>C. Ronchi and J.-P. Hiernaut, *J. Alloys Compd.* **240**, 179 (1996).
- <sup>29</sup>W. A. Lambertson, M. H. Mueller, and F. H. Gunzel, *J. Am. Ceram. Soc.* **36**, 397 (1953).
- <sup>30</sup>R. E. Latta and R. E. Fryxell, *J. Nucl. Mater.* **35**, 195 (1970).
- <sup>31</sup>L. Lyon and E. Bailly, *J. Nucl. Mater.* **22**, 332 (1967).
- <sup>32</sup>C. Guéneau, A. Chartier, and L. V. Brutzel, "Thermodynamic and thermophysical properties of the actinide oxides," in *Comprehensive Nuclear Materials*, 1st ed., edited by R. J. M. Konings (Elsevier, Amsterdam, 2012).
- <sup>33</sup>E. Shapiro, *J. Am. Chem. Soc.* **74**, 5233 (1952).
- <sup>34</sup>P. Kleinschmidt and J. W. Ward, *J. Less-Common Met.* **121**, 61 (1986).
- <sup>35</sup>R. W. Ohse, *J. Chem. Phys.* **44**, 1375 (1966).
- <sup>36</sup>R. J. M. Konings, O. Beneš, A. Kovács, D. Manara, D. Sedmidubsky, L. Grokhov, V. S. Iorish, and V. Yungman, "The thermodynamic properties of the f-elements and their compounds. Part II. The Lanthanide and Actinide Oxides," to be submitted.
- <sup>37</sup>R. J. Ackermann, R. L. Faircloth, and M. H. Rand, *J. Phys. Chem.* **70**, 3698 (1966).